NJC

New Journal of Chemistry

An international journal of the chemical sciences

www.rsc.org/njc

Volume 34 | Number 3 | March 2010 | Pages 369–572

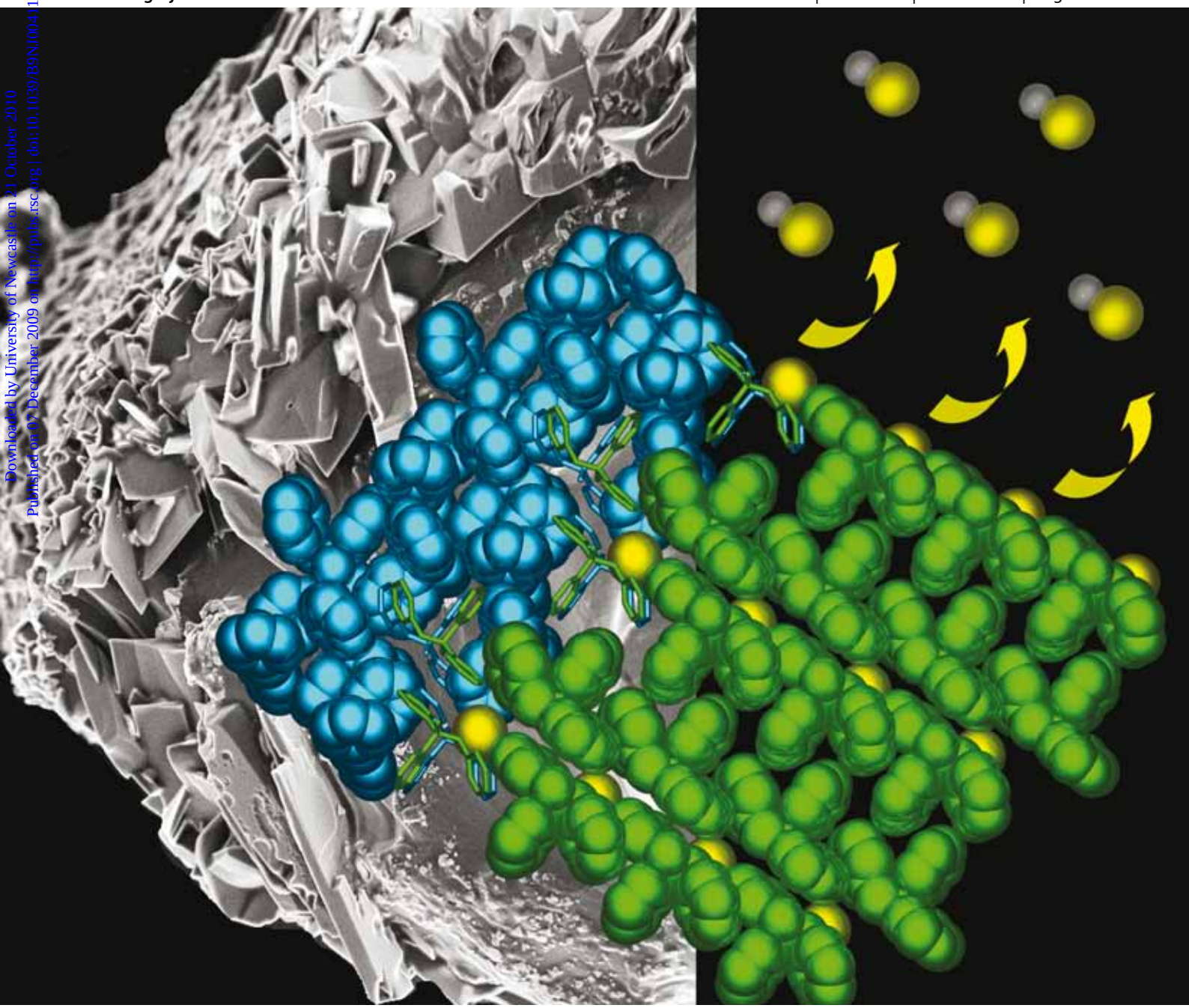

ISSN 1144-0546

RSC Publishing

PAPER

Nikoletta B. Báthori *et al.*

Investigation of sublimation with and without dissociation in the chloride and nitrate salts of 4-(1-hydroxy-1,2-diphenylethyl)pyridine

1144-0546(2010)34:3;1-P

Investigation of sublimation with and without dissociation in the chloride and nitrate salts of 4-(1-hydroxy-1,2-diphenylethyl)pyridine†

Nikoletta B. Báthori,*[a] Petra Bombicz,[b] Susan A. Bourne*[a] and Gerhard A. Venter[a]

Received (in Victoria, Australia) 18th August 2009, Accepted 26th October 2009
First published as an Advance Article on the web 7th December 2009
DOI: 10.1039/b9nj00411d

We observed sublimation–dissociation and recrystallization under ambient pressure when a single crystal of $\mathbf{1H^+ \cdot Cl^-}$ (4-(1-hydroxy-1,2-diphenylethyl)pyridinium chloride) was heated. The native organic moiety (**1**) crystallized on the mother crystal on distinct surfaces, providing an excellent example of molecular structure–macroscopical property relationship which can be explained by partial isostructurality. Under similar conditions the nitrate salt of the same compound, $\mathbf{1H^+ \cdot NO_3^-}$ (4-(1-hydroxy-1,2-diphenylethyl)pyridinium nitrate), sublimed and recrystallized without dissociation. The two crystal structures of the salts are isostructural, but Hirshfeld surface analysis shows significant differences between the intermolecular interactions which explain their different thermal behavior in the crystalline phase. Computational studies in the gas phase provide a theoretical understanding of the solid state behavior.

1. Introduction

Reactions involving no solvent have generated enormous interest in recent years. Most often these studies involve synthetic reactions requiring the close contact of reactants in mechanochemical grinding,[1] "solvent-drop" grinding[2] or microwave-promoted reactions.[3] In some instances, reactions also proceed by the interaction of vapors with the solid state.[4] A major advantage of these types of reactions is the reduced amount of waste from solvent and the increased likelihood of pure products. At the same time, sublimation‡ is one of the simplest techniques used to purify compounds but its mechanism is not always well-understood. Several authors have investigated the kinetics of the sublimation of common industrial salts like ammonium chloride[5] and ammonium perchlorate.[6] Recently Zhu *et al*. used first-principle studies to suggest that sublimation–dissociation reactions of these salts involve a multistage process which includes surface reconstruction of the crystal/bulk material, proton transfer between the ion pairs, desorption from the relaxed surface to gas phase as an ion pair and dissociation to neutral molecules.[7] If the dissociation energy is high enough and recrystallization takes place before dissociation, sublimation can produce crystals which are suitable for single-crystal diffraction.

Understanding of these processes to derive the appropriate structure–property relationships requires careful consideration of crystal morphology and structure. Such understanding is of increasing importance in pharmaceutical research.[8] A number of papers have appeared in the recent literature describing crystal to crystal transformations: for example, the thermochromic compound, 1,5-bis(hydroxyethylamino)-2,4-dinitrobenzene (BDB), exists in two crystalline forms which differ in their hydrogen bonding networks. The thermochromic transformation from one form to the other is reversible and can be followed by X-ray diffraction and DSC.[9] Kepert *et al*. could correlate the transition from ferromagnetic to antiferromagnetic behavior with the dehydration–hydration reaction in a coordination framework.[10] The removal and readsorption of guest molecules was responsible for the crystal transformation in 2D coordination networks of $[Co(NCS)(3\text{-pia})_2]$ (3-pia is *N*-(3-pyridyl)isonicotinamide) which could be followed by EPR and IR spectroscopy.[11] These authors did not correlate the structural changes they describe with crystal morphology. Some other recent papers contain attempts to relate structural transformation to macroscopic morphology but these papers discuss the desolvation process of a single crystal or solvation of a microcrystalline powder and the process was followed by powder X-ray diffractometry only.[12]

The hydrochloride salt of 4-(1-hydroxy-1,2-diphenylethyl)-pyridine, **1** (Scheme 1), provided a useful platform on which to study the progress of a sublimation–decomposition reaction *in situ*. We report here a study of the crystal structure of 4-(1-hydroxy-1,2-diphenylethyl)pyridinium chloride, $\mathbf{1H^+ \cdot Cl^-}$, in which we observed that, on heating to sublimation at ambient pressure, new crystals grow preferentially on certain faces of the mother crystal. The nitrate salt of the same compound, $\mathbf{1H^+ \cdot NO_3^-}$, also sublimes with an accompanying

[a] *Centre for Supramolecular Chemistry Research, Department of Chemistry, University of Cape Town, Rondebosch 7701, South Africa. E-mail: nikoletta.bathori@uct.ac.za, susan.bourne@uct.ac.za; Fax: +27-21-6505195; Tel: +27-21-6502563*
[b] *Institute of Structural Chemistry, Hungarian Academy of Sciences, Pusztaszeri út 59-67, Budapest, Hungary*

† Electronic supplementary information (ESI) available: Thermogravimetric data, powder X-ray traces and crystallographic information for structures **1**, $\mathbf{1H^+ \cdot Cl^-}$ and $\mathbf{1H^+ \cdot NO_3^-}$. CCDC reference numbers 666826 (**1**), 666827($\mathbf{1H^+ \cdot Cl^-}$) and 743052 ($\mathbf{1H^+ \cdot NO_3^-}$). For ESI and crystallographic data in CIF or other electronic format see DOI: 10.1039/b9nj00411d

‡ Sublimation is the term used when matter undergoes phase transition directly from solid to gaseous form or vapor, without passing through the common liquid phase between the two. When it has been used for purification we expect a surface where the matter will recrystallize.

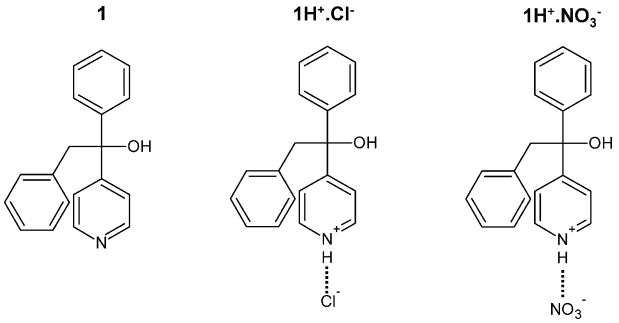

Scheme 1

solid-phase transition on heating. The crystal structures of the two salts are isostructural but the Hirshfeld surface analysis shows significant differences in the intermolecular interactions.

2. Experimental section

2.1 Crystal growth

Compound **1** was obtained from Prof. Edwin Weber of the University of Freiberg, Germany. All reagents and solvents were purchased from Aldrich and used without further purification. The salts reported here were obtained serendipitously in the course of a coordination experiment. The crystals of $\mathbf{1H^+ \cdot Cl^-}$ were grown by slow evaporation of the solvent from a methanol solution of $HAuCl_4$ and compound **1**. The crystals of **1** were grown by sublimation of $\mathbf{1H^+ \cdot Cl^-}$ while crystals of $\mathbf{1H^+ \cdot NO_3^-}$ were obtained by slow evaporation from methanol solution of $FeNO_3 \cdot 12H_2O$.

2.2 Hot stage microscopy (HSM)

Hot stage microscopy experiments were performed using a Linkam THMS600 hot stage mounted on a Nikon SMZ-10 microscope which in turn is fitted with a Sony Digital Hyper HAD color video camera. The temperature was controlled by a Linkam CO600 temperature controller. All samples were subjected to a heating rate of 10 K min^{-1}.

2.3 Thermogravimetry (TG)

Thermogravimetric measurements were performed using a Mettler Toledo TGA/sDTA 851e system under dry N_2 gas purge with a flow rate of 30 ml min^{-1} with a constant scanning rate of 10 K min^{-1}.

2.4 Differential scanning calorimetry (DSC)

The DSC measurements were performed using a Perkin Elmer PC-7 thermal analysis system under dry N_2 gas purge with a flow rate of 30 ml min^{-1} with a constant scanning rate of 10 K min^{-1}.

2.5 Scanning electron microscopy (SEM)

A Leica/LEO Stereoscan S440 fully analytical scanning electron microscope with secondary (SE1) and backscatter detector was used with a working distance of between 40 and 18 mm.

2.6 Powder X-ray diffraction (PXRD)

Powder X-ray diffraction (HUBER Guinier 670 Imaging Plate diffractometer with CuKα radiation 1.5406 Å) at $T = 293$ K established that the bulk material had the same crystal structure as the crystals selected for single-crystal analysis. See ESI† for PXRD traces.

2.7 Single-crystal X-ray diffraction

Crystallographic data of compounds **1**, $\mathbf{1H^+ \cdot Cl^-}$ and $\mathbf{1H^+ \cdot NO_3^-}$ are shown in Table 1.

All data for crystal structure determinations were collected on a Nonius Kappa CCD Single-Crystal X-ray Diffractometer, using graphite monochromated MoKα radiation (λ = 0.7107 Å, $T = 173$ K) generated by a Nonius FR590 generator at 50 kV and 30 mA. The unit cell was indexed from the first 10 frames, and positional data were refined along with diffractometer constants to give the final cell parameters. The strategy for data collection was evaluated using COLLECT software.[13] Integration and scaling with DENZO and SCALEPACK[14] resulted in unique datasets corrected for Lorentz polarization effects and for the effects of crystal decay and absorption by a combination of averaging of equivalent reflection and overall volume and scaling correction. Absorption correction was done empirically using SADABS on the dataset of $\mathbf{1H^+ \cdot Cl^-}$.[15] Accurate unit cell parameters were refined on all data. The structures were solved using SHELXS-97 and refined using full-matrix least-squares methods in SHELXL-97[16] with the aid of the program X-Seed.[17] Non-hydrogen atoms were modeled anisotropically. Hydrogens atoms on carbon atoms were assigned an isotropic thermal parameter 1.2 or 1.5 times that of their parent atom and refined using a riding model. Hydrogen atoms on hydroxyl and pyridyl groups were located in the difference electron density maps and included in a riding model. The analysis of short contacts was carried out using PLATON.[18]

2.8 Isostructurality calculations

The following indices were used for comparison of structures: (i) cell similarity index: $\Pi = [(a + b + c)/(a' + b' + c')] - 1$, where a, b, c and a', b', c' are the orthogonalized lattice parameters of the related crystals.[19] In the event of great similarity of the two unit cells π is close to zero. (ii) Mean elongation: $\varepsilon = (V'/V)^{1/3} - 1$, which describes the difference in cell size, while (iii) asphericity index: $A = (2/3)[1 - \Sigma_{j>i}\{[(1 + \varepsilon)M_i - 1] \times [(1 + \varepsilon)M_j - 1]/3\varepsilon^2\}^{1/2}]$ accounts for the shape distortion (εA is called the lattice distortion index).[20] In the event of great similarity of the two unit cells ε and A are both close to zero. (iv) Isostructurality index: $I_i(n) = [1 - (\Sigma \Delta R^2_i/n)^{1/2}] \times 100\%$. $I_i(n)$ takes into account both the differences in the geometry of the molecules and the positional differences caused by rotation and translation.[21] The isostructurality index for $\mathbf{1H^+ \cdot Cl^-}$ and $\mathbf{1H^+ \cdot NO_3^-}$ was calculated for 22 heavy atoms in each molecule. (v) Volumetric isostructurality index: $I_v = [2V_0/(V_1 + V_2)] \times 100\%$, expressed as the ratio of volume overlap to the average volume. In the event of great similarity of the two unit cells I_v is close to 100%, (vi) $I_v^{max} = [(2\min\{V_1, V_2\})/(V_1 + V_2)] \times 100\%$ when $V_1 \neq V_2$ is the theoretical maximum of I_v.

Table 1 Crystallographic data of compound **1**, $\mathbf{1H^+ \cdot Cl^-}$ and $\mathbf{1H^+ \cdot NO_3^-}$

	1	$\mathbf{1H^+ \cdot Cl^-}$	$\mathbf{1H^+ \cdot NO_3^-}$
Crystal data			
CCDC no.	666826	666827	743052
Chemical formula	$C_{19}H_{17}NO$	$C_{19}H_{18}NOCl$	$C_{19}H_{18}N_2O_4$
Formula weight	275.34	311.80	338.35
Temperature/K	173	173	173
Crystal system	Monoclinic	Triclinic	Triclinic
Space group (no.)	$P2_1/c$ (no. 14)	$P\bar{1}$ (no. 2)	$P\bar{1}$ (no. 2)
a/Å	9.3446(19)	6.3219(13)	6.3168(13)
b/Å	10.612(2)	8.4477(17)	8.1971(16)
c/Å	15.267(3)	15.349(3)	16.497(3)
α/°	90.00	102.22(3)	100.78(3)
β/°	107.70(3)	92.54(3)	91.20(3)
γ/°	90.00	106.21(3)	100.44(3)
V/Å^3	1442.2(5)	764.6(3)	823.9(3)
Z'/Z	1/4	1/2	1/2
D_{calc}/Mg m^{-3}	1.268	1.354	1.364
Radiation type	MoKα	MoKα	MoKα
μ/mm^{-1}	0.078	0.251	0.097
F(000)	584	328	356
Crystal size/mm	0.4 × 0.4 × 0.3	0.5 × 0.5 × 0.5	0.1 × 0.1 × 0.1
Color, crystal form	Rods, colorless	Prism, colorless	Prism, colorless
Data collection			
Absorption correction	None	Multi-scan	None
T_{min}/T_{max}	—	0.879/0.882	—
Number of measured, unique reflections	30 355/2835	12 756/3103	3025/1900
R(int)	0.067	0.032	0.0789
$\Theta_{min-max}$/°	2.4–26.0	3.2–26.3°	3.23–25.63
Refinement			
$R[F^2 > 2\sigma(F^2)]$, w$R(F^2)$, S	0.0370/0.0932/1.04	0.0333/0.0895/1.04	0.0501/0.1181/1.04
No. of reflections	2835	3103	3025
No. of parameters	192	208	229
Max. and average shift/esd	0.000/0.000	0.000/0.000	0.000/0.000
Res. peak max/min/e Å^{-3}	–0.19, 0.17	–0.22, 0.27	–0.20, 0.4

2.9 Computational details

Initial calculations at B3LYP/6-31 + G(d,p) were performed to optimize the structures of the $\mathbf{1H^+ \cdot Cl^-}$ and $\mathbf{1H^+ \cdot NO_3^-}$ complexes. A reduction in the complexity of the electronic structure calculation was sought by representing the organic part of the complex with a simplified system of tertiary butanol, optimized at the same level of theory. The effect of this simplification was evaluated by comparison of the change in the DFT electron density distribution, through calculation of Mulliken partial atomic charges, on the C7–O8–H8 series of centers. The partial charges on the oxygen atoms (O8) are similar at −0.362 e and −0.374 e for $\mathbf{1 \cdot H^+}$ and tertiary butanol, respectively. That on H8 decreases from 0.368 e to 0.231 e on replacing the aromatic rings with methyl groups. This change in partitioning is balanced by the carbon atom C7, whose charge increases from 0.161 e to 0.292 e, leaving the combined charge on the whole COH group in both cases very similar. The change in C7 partial atomic charge can be explained by the electron withdrawing nature of the aromatic substituents, as opposed to the electron releasing nature of the methyl groups. In conclusion, we are satisfied that using tertiary butanol to mimic the full complex is an acceptable simplification.

For the determination of the interaction energies, geometries of the tertiary butanol chloride–nitrate complexes were optimized using density functional theory at the B3LYP/6-311 + G(2df,2p) level. Subsequent single point energies were conducted using coupled cluster theory, at the CCSD(T)/6-311 + G(2df,2p) level. The dissociation energy, D_e, was determined at the same level of coupled cluster theory from relaxed structures at B3LYP/6-311 + G(2df,2p). The Gaussian 03 software package was used for all quantum mechanical calculations.[22]

3. Results and discussion

In this study we found two simple salts of 4-(1-hydroxy-1,2-diphenylethyl)pyridine, **1**, which both sublime but then differ in their behavior in the gas phase. While $\mathbf{1H^+ \cdot NO_3^-}$ retains its identity and recrystallizes as the identical salt, $\mathbf{1H^+ \cdot Cl^-}$ decomposes in the gas phase into its constituent parts and the recrystallized product is **1**. Moreover, the recrystallization of **1** can be observed to occur on large crystals of $\mathbf{1H^+ \cdot Cl^-}$ but occurs preferentially on equivalent faces of the mother crystal. Thermal analysis and scanning electron microscopy allowed us to follow this process and to correlate the reaction with the crystal morphology.

3.1 Single-crystal studies of compound 1, $\mathbf{1H^+ \cdot Cl^-}$ and $\mathbf{1H^+ \cdot NO_3^-}$ and isostructurality calculations

Bond lengths and angles of the 4-(1-hydroxy-1,2-diphenylethyl)pyridine are similar in the three structures. Apart from the protonation of the pyridyl nitrogen, which hydrogen bonds to the chloride or nitrate ion (in $\mathbf{1H^+ \cdot Cl^-}$ and $\mathbf{1H^+ \cdot NO_3^-}$, respectively), the only significant difference between the structures is the relative orientation of the benzyl group (Fig. 1). The torsion angle C16–C7–C9–C10 is 178.75(11)° in **1**,

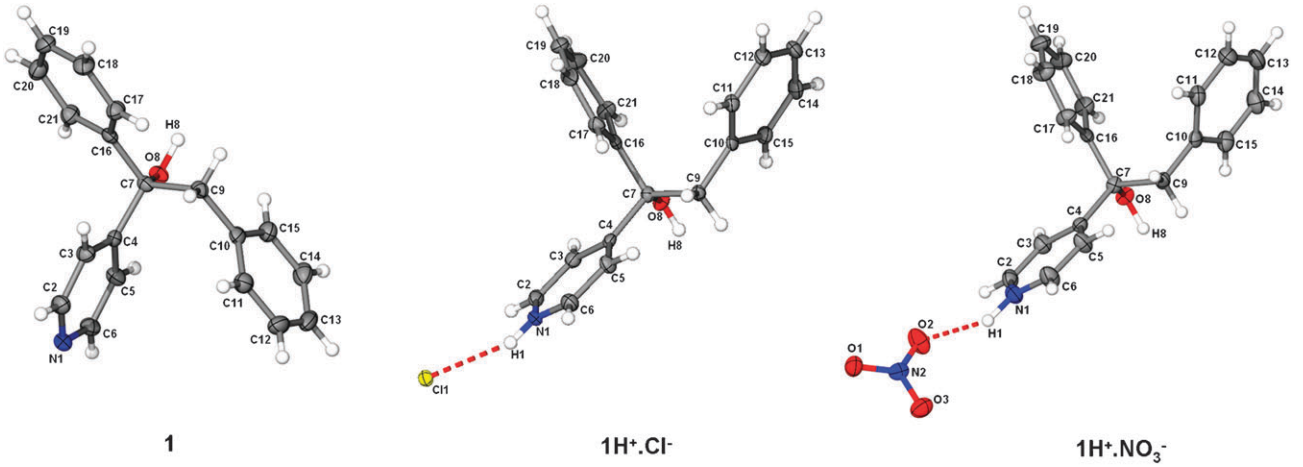

Fig. 1 ORTEP diagrams of 4-(1-hydroxy-1,2-diphenylethyl)pyridine (**1**) and its chloride ($\mathbf{1H^+ \cdot Cl^-}$) and nitrate salts ($\mathbf{1H^+ \cdot NO_3^-}$). The thermal ellipsoids drawn at 50% probability level and H atoms are shown as spheres of arbitrary radius.

50.40(4)° in $\mathbf{1H^+ \cdot Cl^-}$ and 53.6(3)° in $\mathbf{1H^+ \cdot NO_3^-}$ giving a folded conformation in the salts.

In the crystal structure of **1** the molecules are connected into head-to-tail chains with O8–H8···N1 (O8···N1 = 2.851(1) Å) hydrogen bonding (Fig. 2). These chains are connected through weak C13–H13···O8 (C13···O8 = 2.708(2) Å) intermolecular interactions. Crystals of $\mathbf{1H^+ \cdot Cl^-}$ consist of hydrogen-bonded chains of molecules, linked by pyridine N1–H1···Cl1 (N1···Cl1 = 3.388(2) Å) and hydroxyl O8–H8···Cl1 (O8···Cl1 = 3.098(1) Å) interactions which run parallel to [010] (Fig. 3). There are π···π interactions between the pyridine rings with a distance between the offset parallel planes of 3.63 Å. Adjacent chains of molecules have interdigitated phenyl and benzyl groups forming a zipper motif. The crystal structure of $\mathbf{1H^+ \cdot NO_3^-}$ has the same packing motif as in $\mathbf{1H^+ \cdot Cl^-}$ (Fig. 3). The nitrate anion hydrogen bonds through N1–H1···O2 (N1···O2 = 2.892(2) Å) and O8–H8···O1 (O8···O1 = 2.748(2) Å) to the protonated 4-(1-hydroxy-1,2-diphenylethyl)pyridine moiety. However, the distance between the offset parallel planes of pyridine rings is 4.08 Å, significantly longer than in $\mathbf{1H^+ \cdot Cl^-}$. Table 2 lists the intermolecular interactions in all three structures.

The three structures have similar packing coefficients (**1**: 69.1%, $\mathbf{1H^+ \cdot Cl^-}$: 71.9%, $\mathbf{1H^+ \cdot NO_3^-}$: 70.4%). The unit cell similarity (Π = 0.0341), the lattice distortion index (εA = 0.0397) and the isostructurality indices ($I_i(22)$ = 67.9%, I_v = 90.6%, $I_{v,max}$ = 97.2% and calculated only for the organic components: $I_i(21)$ = 68.9%, I_v = 91.8%, $I_{v,max}$ = 97.2%) indicate that the two crystal structures show a high level of isostructurality.

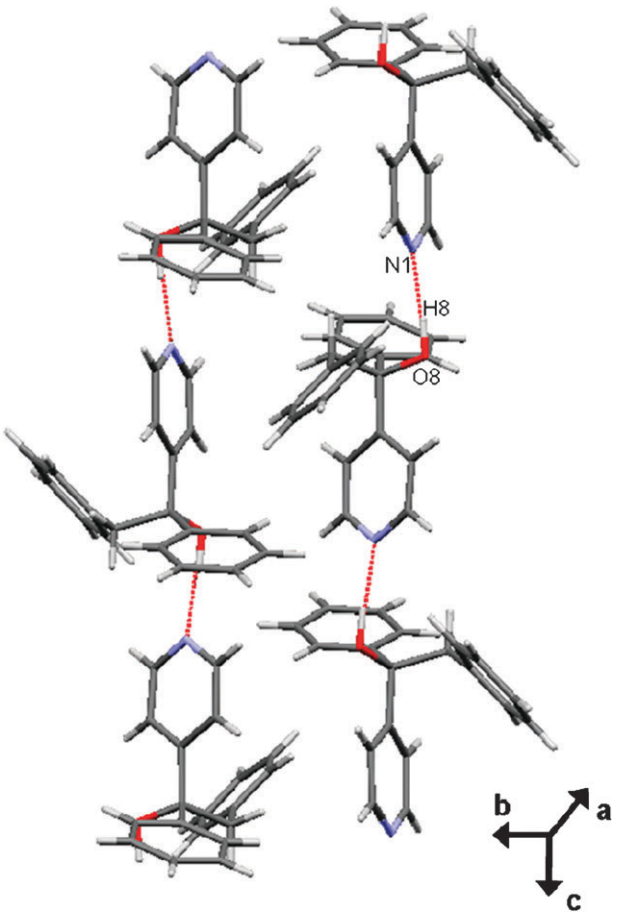

Fig. 2 Hydrogen bonds in structure **1**.

3.2 Thermoanalytical studies

Differential scanning calorimetry (DSC) showed significant differences between the three compounds (Fig. 4). Interpretation of DSC was aided by following the thermal processes using hot stage microscopy (HSM). The crystals of **1** melt at 190 °C while crystals of $\mathbf{1H^+ \cdot Cl^-}$ start to sublime at *ca.* 180.5 °C and to decompose at *ca.* 250 °C. DSC of crystals of $\mathbf{1H^+ \cdot NO_3^-}$ shows an endothermic peak at 216 °C and an exothermic peak at 218 °C, the latter attributable to recrystallization. Crystals of $\mathbf{1H^+ \cdot NO_3^-}$ decompose at 300 °C. The thermogravimetry (TG) of **1** and $\mathbf{1H^+ \cdot Cl^-}$ are featureless, indicating that neither of the two crystals includes solvent. The TG trace of crystals $\mathbf{1H^+ \cdot NO_3^-}$ also shows no indication of solvent inclusion. There is a broad initial mass loss attributed to the drying of surface solvent. (For TG curves see ESI†.)

For hot stage microscopy we placed the crystal between two cover slips separated by a spacer to allow a suitable distance for the sublimation to occur. As it was heated, the crystal of

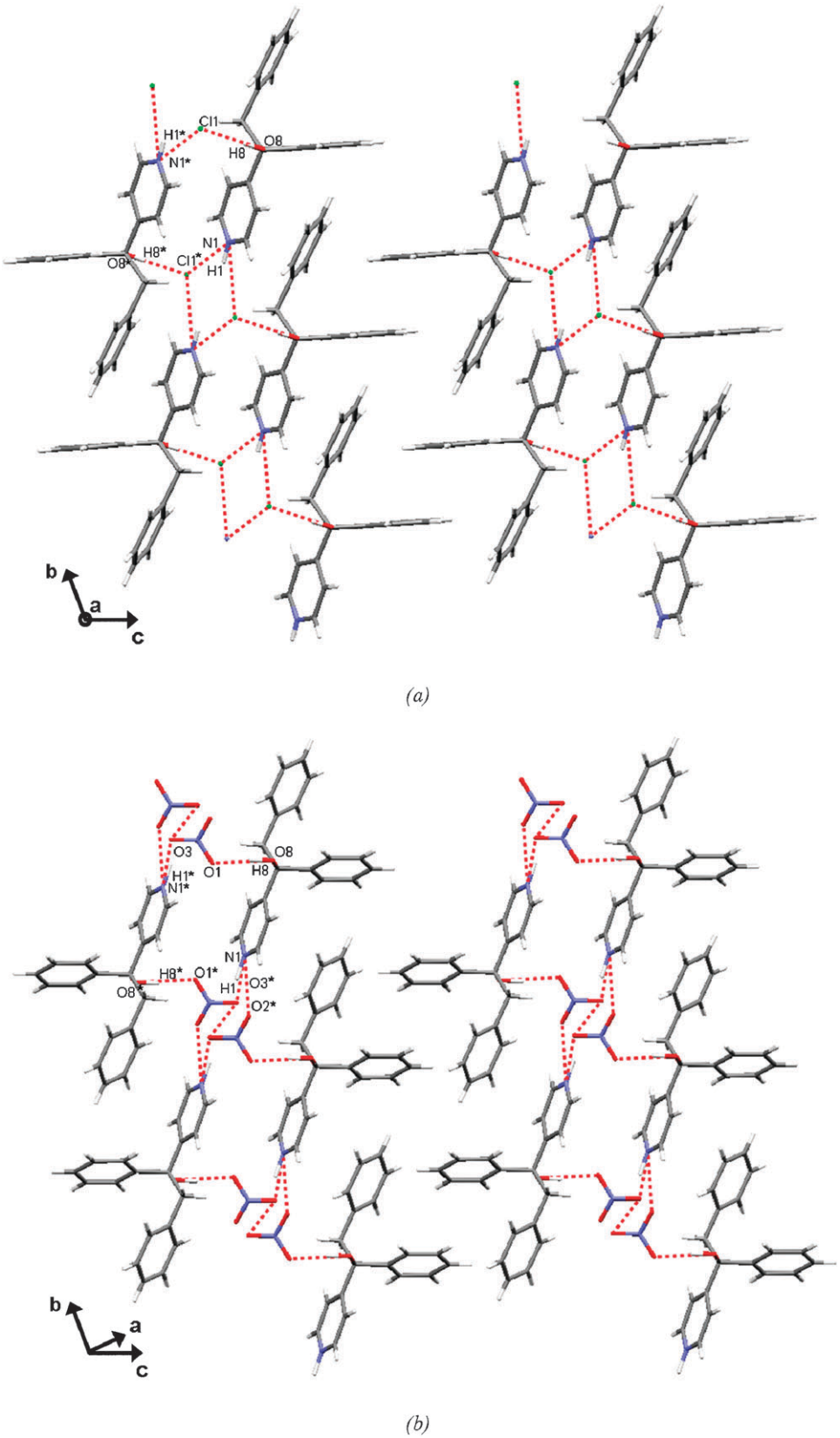

Fig. 3 Hydrogen bonds in structure $\mathbf{1H^+ \cdot Cl^-}$ (a) and $\mathbf{1H^+ \cdot NO_3^-}$ (b).

$\mathbf{1H^+ \cdot Cl^-}$ (1.375 mm × 0.937 mm × 0.375 mm) became opaque and began to sublime at *ca.* 180 °C (Fig. 5A). After 5 minutes a significant amount of product (**1**) had crystallized onto the top cover slip. These crystals were unsuitable for single-crystal

Table 2 Hydrogen bonding in crystal **1**, $\mathbf{1H^+ \cdot Cl^-}$ and $\mathbf{1H^+ \cdot NO_3^-}$

D–H···A	D–H/Å	D···A/Å	H···A/Å	D–H···A/°
1				
O8–H8···N1^{*,a}	0.96	2.851(2)	1.89	175
$\mathbf{1H^+ \cdot Cl^-}$				
O8–H8···Cl1	0.86	3.098(1)	2.25	170
N1–H1···Cl1^{*,b}	0.85	3.140(2)	2.40	144
N1–H1···Cl1^{*,c}	0.85	3.388(2)	2.82	125
C14–H14···C$_{g,a}$	0.95	3.739(1)	3.23	47^f
$\mathbf{1H^+ \cdot NO_3^-}$				
O8–H8···O1	1.01	2.748(2)	1.75	173
N1–H1···O2^{*,d}	1.08	2.892(2)	2.10	129
N1–H1···O3^{*,e}	1.08	3.000(3)	2.21	129
C14–H14···C$_{g,a}$	0.95	3.798(3)	3.15	55^f

*Symmetry operators:^{a} $x, 1/2 - y, 1/2 + z$. ^{b} $-1 + x, -1 + y, z$. ^{c} $-x, 1 - y, -z$. ^{d} $1 + x, 1 + y, z$. ^{e} $2 - x, 2 - y, 1 - z$. ^{f} Interplanar angle between L.S. planes of ring a and b (a = N1–C2–C3–C4–C5–C6, b = C10–C11–C12–C13–C14–C15).

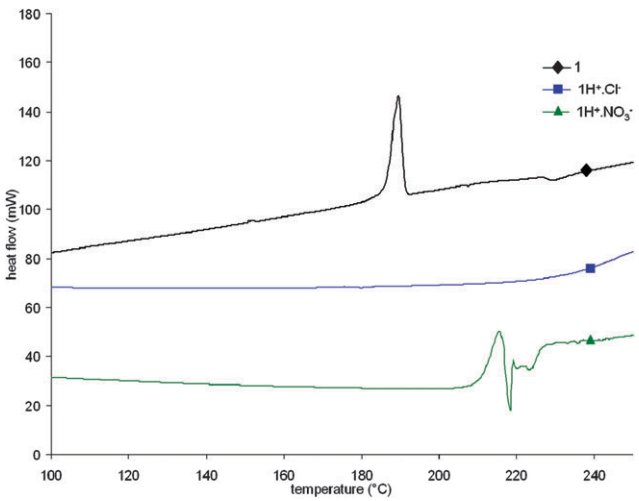

Fig. 4 DSC results of compounds **1**, $\mathbf{1H^+ \cdot Cl^-}$ and $\mathbf{1H^+ \cdot NO_3^-}$ showing their different thermal stabilities.

X-ray diffraction. In order to obtain crystals of good quality we kept the mother crystal at 200 °C for 30 minutes which produced large, good quality crystals for single-crystal X-ray diffraction (Fig. 5B). These columnar crystals grow on the surface of the mother crystal; they could be subjected to DSC and single-crystal XRD which confirmed that they are crystals of compound **1**.

HSM results showed that the crystal of $\mathbf{1H^+ \cdot NO_3^-}$ changed opacity rapidly between 190–200 °C while it was heated, which indicates a phase transition/recrystallization process. From the top cover slip we collected some crystals which were suitable for single-crystal X-ray diffraction.

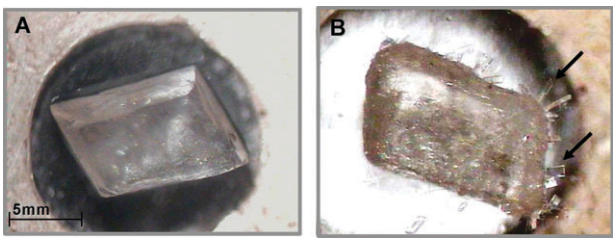

Fig. 5 HSM pictures of the sublimation–decomposition process. A crystal of $\mathbf{1H^+ \cdot Cl^-}$ before heating (note prismatic morphology). The crystal became opaque at *ca.* 180 °C (A). Maintaining the temperature at 200 °C for 30 minutes allows crystals of **1** to grow on the surface of the mother crystal ($\mathbf{1H^+ \cdot Cl^-}$). Black arrows indicate the columnar crystals of **1** which could be subjected to single-crystal X-ray diffraction (B).

3.3 Crystal transformation studies

In order to study the crystal transformation of $\mathbf{1H^+ \cdot Cl^-}$ to **1**, we selected a large crystal (8 × 3 × 1.5 mm) to perform SEM analysis. After subjecting this crystal to the sublimation process by heating it at 200 °C for 30 minutes, SEM pictures were taken to determine the main direction of growth for the new crystals of **1** (Fig. 6A). On the top surface and the long side of the mother crystal we did not observe significant crystal growth while on the short side many small crystals are apparent.

Perpendicular to the cut direction, the crystal was broken and this new surface was perfectly smooth (Fig. 6B). To identify the crystal growth surface we used BFDH morphology prediction[23] which agrees well with the crystal shape and the face indexing performed on a single crystal of $\mathbf{1H^+ \cdot Cl^-}$ (Fig. 6C).

These results show the chloride-layer of the crystal as being parallel with the top surface ((001) plane). We propose a mechanism for the reaction of $\mathbf{1H^+ \cdot Cl^-}$ to **1** according to Zhu *et al.* as follows: (i) sublimation of $\mathbf{1H^+ \cdot Cl^-}$ by the breaking of weak intermolecular interactions between phenyl and benzyl groups ('unzipping'), from the (001) and (00−1) planes; (ii) loss of HCl(g) in the direction of the (010) and (0−10) planes; (iii) recrystallization of product **1** on the (100) and (−100) planes of the mother crystal. This mechanism is consistent with both the morphology prediction and the observation that no recrystallization occurs on the (001), (00−1) and (010), (0−10) planes.

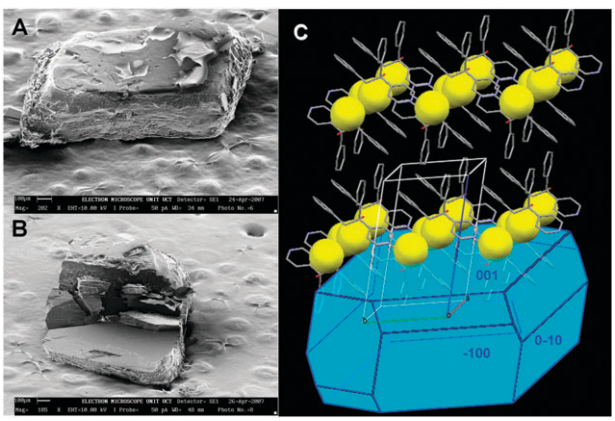

Fig. 6 SEM pictures of $\mathbf{1H^+ \cdot Cl^-}$. A: surface of the mother crystal, on the top surface and the long side which have no new crystal growth. The short side of the mother crystal is crowded by new crystals of compound **1**. B: surface of the mother crystal when broken. C: comparison of the SEM result and the BFDH predicted morphology result of crystal $\mathbf{1H^+ \cdot Cl^-}$.

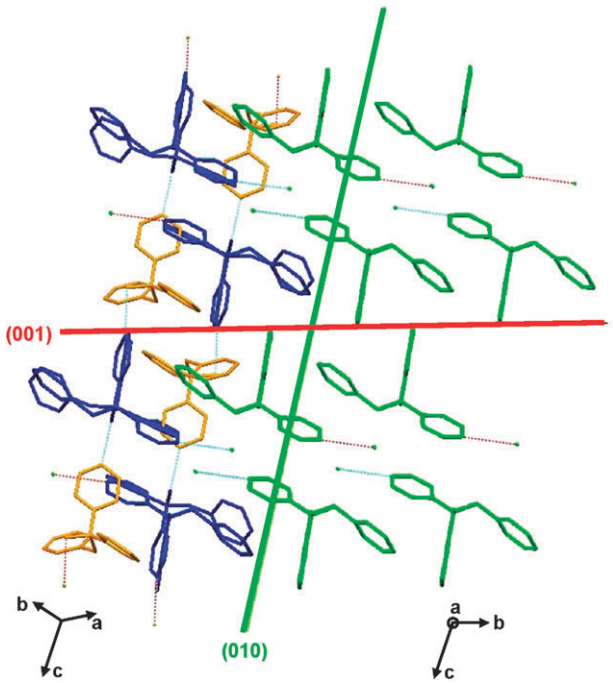

Fig. 7 Superimposed crystal structures of **1** (blue-yellow) and $\mathbf{1H^+ \cdot Cl^-}$ (blue-green) shows a pair of pyridine derivative molecules form the synthon that occurs in both **1** and $\mathbf{1H^+ \cdot Cl^-}$.

A highly similar supramolecular synthon can be recognized in both crystal structures of $\mathbf{1H^+ \cdot Cl^-}$ and **1** formed by a pair of molecules (shown in blue in Fig. 7). With the sublimation and the escape of HCl the type and direction of the strong secondary interactions change. In the sublimate (**1**), the newly formed O–H···N interaction is approximately perpendicular to the original N–H···Cl. This requires a small rearrangement of the molecules in the crystals, although the synthon remains unchanged. The internal arrangement corresponds well with the crystal morphology: $\mathbf{1H^+ \cdot Cl^-}$ are bulky prisms while **1** is columnar. The rather similar *c* cell axes (15.349(3) Å in $\mathbf{1H^+ \cdot Cl^-}$ and 15.267(3) Å in **1**) are parallel along the synthons in the two crystal structures. This partial isostructurality may explain why new crystal columns grow on specific faces (010 and 0−10) of the mother prism and not on other sides of the bulky crystal. When $\mathbf{1H^+ \cdot NO_3^-}$ crystals were heated in a similar fashion, they sublimed and recrystallized on the top cover slip. Although there was insufficient crystalline material for powder X-ray diffraction analysis several crystals were subjected to single-crystal X-ray diffraction. The data quality was poor, but the same structure was indexed, solved and refined in four triclinic unit cells. The cells are not transformable to each other because of the poor quality data but the fitted structure proves the same packing arrangement of the molecules, hence sublimation occurred without decomposition. (The details of the sublimed crystals and the fitted packing diagrams have been shown in ESI†.)

3.4 Comparison of $\mathbf{1H^+ \cdot Cl^-}$ and $\mathbf{1H^+ \cdot NO_3^-}$

Given the different thermal behavior but isostructural crystal structures of the two salts we considered the Hirshfeld surface analysis of $\mathbf{1H^+ \cdot Cl^-}$ and $\mathbf{1H^+ \cdot NO_3^-}$.[24] Fingerprint plots are shown in Fig. 5 where d_e and d_i are defined as the distances from the surface of the nearest atom external and internal to the surface. We generated the Hirshfeld surface of the organic cations (Fig. 8a and b) and the ion pairs when they are hydrogen bonded through the hydroxyl group to the anion (Fig. 8c and d). Comparing the fingerprint plots it is clearly visible that the cations of compound $\mathbf{1H^+ \cdot Cl^-}$ and $\mathbf{1H^+ \cdot NO_3^-}$ show a similar asymmetric arrangement of interactions because of their identical hydrogen donor features. Comparison of H···Cl^- (spike①) and H···NO_3^- (spike ②) interactions of the cations shows only significant differences in their lengths while the 'chicken wing' (③) on the fingerprint plot of $\mathbf{1H^+ \cdot NO_3^-}$ indicates prominent C–H···π interactions between the aromatic rings. Comparing the fingerprint plots of the cation to the ion pair in structure $\mathbf{1H^+ \cdot Cl^-}$ (Fig. 8a and c) the differences are not remarkable, the shape of the plots are very similar, the extra spike is related to the hydrogen bond acceptor feature of the ion pair and there is no significant difference between the length of the hydrogen bonds (①). The remarkable difference between the fingerprint plots of the nitrate salt (Fig. 8b and d) is the increasing H···NO_3^- distance. The greater difference observed between Fig. 8b and d implies that the $\mathbf{1H^+ \cdot NO_3^-}$ pair is more cohesive and interacts less strongly with the external environment (procrystal). Hence we expect that this ion pair will be more stable than $\mathbf{1H^+ \cdot Cl^-}$.

3.5 Computational results of gas phase behavior

The interaction of the chloride and nitrate ion with the hydroxyl hydrogen of O8 was analyzed in order to investigate the strength of dissociation of one of these protonated species from the organic complex. Interaction between the N1 hydrogen with the anions was not considered, as this was deemed to be the stronger interaction due to the increased electrostatic component resulting from the pyridyl moiety being protonated, and therefore not the energetically limiting step in the dissociation. We used a simplified representation of the complex where the phenyl, benzyl and pyridyl rings were substituted by methyl groups, to give uncharged tertiary butanol. The validity of this approximation was shown by comparison of the electron density (through Mulliken atomic partial charges) at the C7–O8–H8 centers using both the full cationic complex and the resultant neutral simplified species. Details of the findings are given in the Experimental section on Computational details.

The Cl^-···HO hydrogen bond (–19.9 kcal mol^{-1}) is stronger than the O2N–O^-···H–O interaction (–17.1 kcal mol^{-1}) by 2.8 kcal mol^{-1}. Although the chloride anion is a weaker hydrogen bond acceptor than nitrate, it is smaller and has a higher charge density, giving overall larger interaction strength due to the enhanced electrostatic interaction. This stronger interaction is also reflected in the dissociation energy of HCl and HNO_3 from *t*-BuOH[Cl]$^-$ and *t*-BuOH[NO_3]$^-$. This process represents the physical behavior that is observed for $\mathbf{1H^+ \cdot Cl^-}$ upon heating of the complex. Dissociation to give HCl and *t*-BuO^- is endothermic requiring 65.4 kcal mol^{-1}. On the other hand, dissociation of *t*-BuOH[NO_3^-] to give *t*-BuO^- and HNO_3 requires 69.3 kcal mol^{-1}. The more favorable dissociation of HCl, which can in part be substantiated by

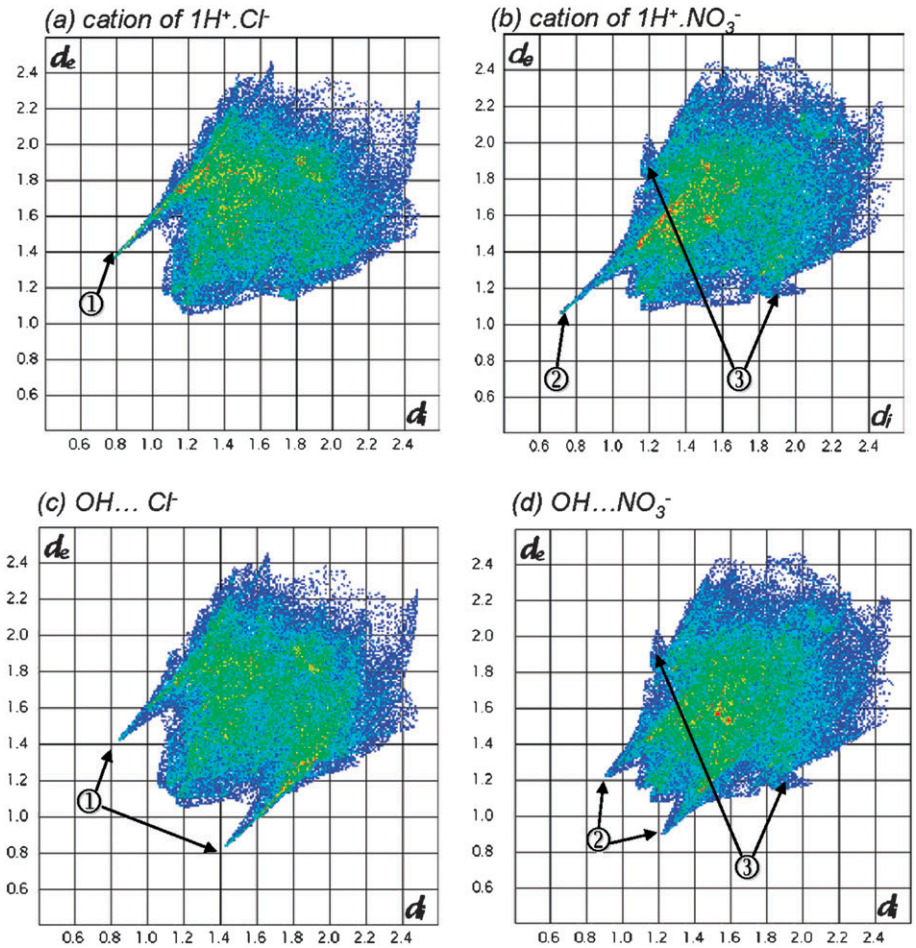

Fig. 8 2D fingerprint plots of cations of $\mathbf{1H^+\cdot Cl^-}$ (a) and $\mathbf{1H^+\cdot NO_3^-}$ (b) and the ion pairs when they are hydrogen bonded through the hydroxyl group to the anion: (c) OH···Cl^- in $\mathbf{1H^+\cdot Cl^-}$ and (d) OH···ONO_2^- in $\mathbf{1H^+\cdot NO_3^-}$.

the stronger affinity of chloride for the hydroxyl hydrogen, lies at the heart of the observed dissociation–sublimation of HCl and recrystallization of the organic complex that is observed for $\mathbf{1H^+\cdot Cl^-}$.

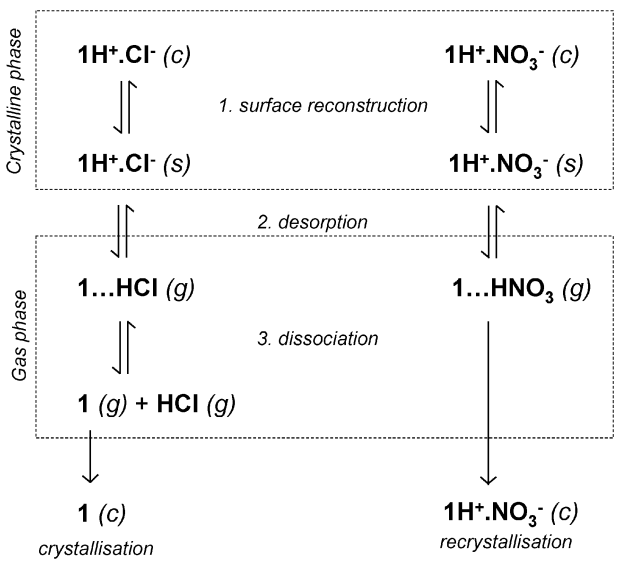

Fig. 9 Schematic diagram of the thermal behavior of $\mathbf{1H^+\cdot Cl^-}$ and $\mathbf{1H^+\cdot NO_3^-}$. (c refers to crystal environment, s refers to relaxed surface, g refers to the gas phase.)

4. Conclusion

To summarize the thermal behavior of the two salts (Fig. 9, c refers to crystal environment, s refers to relaxed surface, g refers to the gas phase) the proposed reaction scheme for the sublimation–decomposition reaction of crystals of $\mathbf{1H^+\cdot Cl^-}$ is the following: (1) $\mathbf{1H^+\cdot Cl^-_{(c)}}$ ion pair gets to the relaxed surface (001, 00−1) of the crystal $\mathbf{1H^+\cdot Cl^-_{(s)}}$; (2) the ion pair undergoes proton transfer ($\mathbf{1\cdots HCl_{(g)}}$) and desorbs from the surface as a pair $\mathbf{1\cdots HCl_{(g)}}$ and (3) dissociates in gas phase to $\mathbf{1_{(g)}}$ and $\mathbf{HCl_{(g)}}$. The dissociation of $\mathbf{1\cdots HCl_{(g)}}$ can be expected to occur because of the relatively high interaction energy between the hydrogen atom of the OH group and the Cl^- and the relatively low dissociation energy of the $\mathbf{1\cdots HCl_{(g)}}$ ion pair. In the final step **1** will crystallize back to the (100) and (−100) planes of the mother crystal, because the close relation (partial isostructurality) of the dimeric synthon best matches this surface. In the case of the $\mathbf{1H^+\cdot NO_3^-}$ crystal the proposed reaction scheme differs in step (3). The calculated interaction energy of ion pair $\mathbf{1H^+\cdot NO_3^-_{(g)}}$ is lower than in $\mathbf{1\cdots HCl_{(g)}}$ while the dissociation energy of the nitrate ion pair is higher.

Hence crystals of $\mathbf{1H^{+}\cdot NO_3^{-}}$ will sublime and recrystallize without decomposition when they are heated at ambient pressure.

Acknowledgements

The authors thank Ms. Miranda Waldron for the SEM photographs. Financial support has been received from the South African National Research Foundation (Grant FA2006030100003) and the South African-Hungarian intergovernmental project (OMFB-00825/2007). NBB thanks the South African National Research Foundation for a Postdoctoral Fellowship (SPF2005072700016).

Notes and references

1 G. Kaupp, *CrystEngComm*, 2009, **11**, 388.
2 (*a*) D. Braga, S. L. Giaffreda, K. Rubini, F. Grepioni, M. R. Chierotti and R. Gobetto, *CrystEngComm*, 2007, **9**, 39; (*b*) M. C. Etter, S. M. Reutzel and C. G. Choo, *J. Am. Chem. Soc.*, 1993, **115**, 4411.
3 G. Keglevich and E. Dudás, *Synth. Commun.*, 2007, **37**, 3191.
4 (*a*) S. Nakamatsu, S. Toyota, W. Jones and F. Toda, *Chem. Commun.*, 2005, 3808; (*b*) D. Braga, S. L. Giaffreda, F. Grepioni, M. R. Chierotti, R. Gobetto, G. Palladino and M. Polito, *CrystEngComm*, 2007, **9**, 879.
5 (*a*) R. F. Chaiken, D. J. Sibbett, J. E. Sutherland, D. K. Van De Mark and A. Wheeler, *J. Chem. Phys.*, 1962, **37**, 2311; (*b*) O. Knacke, I. N. Stranski and G. Z. Wolff, *Phys. Chem.*, 1951, **198**, 1157.
6 (*a*) J. Davies, P. W. M. Jacobs and A. Russel-Jones, *Trans. Faraday Soc.*, 1967, **63**, 1737; (*b*) P. W. M. Jacobs and A. Russel-Jones, *J. Phys. Chem.*, 1968, **72**, 202.
7 (*a*) R. S. Zhu, J. H. Wang and M. C. Lin, *J. Phys. Chem. C*, 2007, **111**, 13831–13838; (*b*) R. S. Zhu and M. C. Lin, *J. Phys. Chem. C*, 2008, **112**, 14481–14485.
8 S. R. Byrn, R. R. Pfeiffer and J. G. Stowell, *Solid-State Chemistry of Drugs*, SSCI, Inc., West Lafayette, IN, 1999.
9 S. C. Lee, Y. G. Jeong, W. H. Jo, H.-J. Kim, J. Jang, K.-M. Park and I. H. Chung, *J. Mol. Struct.*, 2006, **825**(1–3), 70.
10 M. Kurmoo, H. Kumagai, K. W. Chapman and C. J. Kepert, *Chem. Commun.*, 2005, 3012.
11 K. Uemura, S. Kitagawa, M. Kondo, K. Fukui, R. Kitaura, H.-C. Chang and T. Mizutani, *Chem.–Eur. J.*, 2002, **8**, 3586.
12 (*a*) S. Petit, F. Mallet, M.-N. Petit and G. Coquerel, *J. Therm. Anal. Calorim.*, 2007, **90**, 39–47; (*b*) K. Yoshizawa, S. Toyota and F. Toda, *Tetrahedron*, 2004, **60**, 7767–7774.
13 *COLLECT, Data Collection Software*, Nonius, Delft, The Netherlands, 1999.
14 Z. Otwinowski, W. Minor, *DENZO and SCALEPACK*, in *International Tables of Crystallography*, ed. M. G. Rossman, E. Arnold, Kluwer, Dordrecht, 2000, vol. F.
15 G. M. Sheldrick, *SADABS, Program for area detector adsorption correction*, Institute for Inorganic Chemistry, University of Göttingen, Germany, 1996.
16 G. M. Sheldrick, *SHELXS-97 and SHELXL-97, Programs for crystal structure determination and refinement*, University of Göttingen, Germany, 1997.
17 L. J. Barbour, *J. Supramol. Chem.*, 2000, **1**, 86.
18 A. L. Spek, *J. Appl. Crystallogr.*, 2003, **36**, 7.
19 A. Kálmán, L. Párkányi and G. Argay, *Acta Crystallogr., Sect. B: Struct. Sci.*, 1993, **49**, 1039–1049.
20 J. S. Rutherford, *ACH – Models Chem.*, 1997, **134**, 395–405.
21 L. Fábián and A. Kálmán, *Acta Crystallogr., Sect. B: Struct. Sci.*, 1999, **55**, 1099–1108.
22 M. J. Frisch, G. W. Trucks, H. B. Schlegel, G. E. Scuseria, M. A. Robb, J. R. Cheeseman, J. A. Montgomery, Jr., T. Vreven, K. N. Kudin, J. C. Burant, J. M. Millam, S. S. Iyengar, J. Tomasi, V. Barone, B. Mennucci, M. Cossi, G. Scalmani, N. Rega, G. A. Petersson, H. Nakatsuji, M. Hada, M. Ehara, K. Toyota, R. Fukuda, J. Hasegawa, M. Ishida, T. Nakajima, Y. Honda, O. Kitao, H. Nakai, M. Klene, X. Li, J. E. Knox, H. P. Hratchian, J. B. Cross, V. Bakken, C. Adamo, J. Jaramillo, R. Gomperts, R. E. Stratmann, O. Yazyev, A. J. Austin, R. Cammi, C. Pomelli, J. W. Ochterski, P. Y. Ayala, K. Morokuma, G. A. Voth, P. Salvador, J. J. Dannenberg, V. G. Zakrzewski, S. Dapprich, A. D. Daniels, M. C. Strain, O. Farkas, D. K. Malick, A. D. Rabuck, K. Raghavachari, J. B. Foresman, J. V. Ortiz, Q. Cui, A. G. Baboul, S. Clifford, J. Cioslowski, B. B. Stefanov, G. Liu, A. Liashenko, P. Piskorz, I. Komaromi, R. L. Martin, D. J. Fox, T. Keith, M. A. Al-Laham, C. Y. Peng, A. Nanayakkara, M. Challacombe, P. M. W. Gill, B. Johnson, W. Chen, M. W. Wong, C. Gonzalez and J. A. Pople, *GAUSSIAN 03 (Revision C.02)*, Gaussian, Inc., Wallingford, CT, 2004.
23 C. F. Macrae, P. R. Edgington, P. McCabe, E. Pidcock, G. P. Shields, R. Taylor, M. Towler and J. van de Streek, Mercury: visualization and analysis of crystal structures, *J. Appl. Crystallogr.*, 2006, **39**, 453.
24 (*a*) J. J. McKinnon, M. A. Spackman and A. S. Mitchell, *Acta Crystallogr., Sect. B: Struct. Sci.*, 2004, **60**, 627–668; (*b*) M. A. Spackman and J. J. McKinnon, *CrystEngComm*, 2002, **4**, 378–392; (*c*) J. J. McKinnon, D. Jayatilaka and M. A. Spackman, *Chem. Commun.*, 2007, 3814–3816.